CRYSTAL GROWTH & DESIGN
2006
VOL. 6, NO. 1
197−201

Peptide Controls on Calcite Mineralization: Polyaspartate Chain Length Affects Growth Kinetics and Acts as a Stereochemical Switch on Morphology

S. Elhadj,*,† E. A. Salter,‡ A. Wierzbicki,‡ J. J. De Yoreo,§ N. Han,† and P. M. Dove†

Department of Geosciences, Virginia Tech, Derring Hall, Blacksburg, Virginia 24061, Department of Chemistry, University of South Alabama, Mobile, Alabama 36688, and Department of Chemistry and Materials Science, Lawrence Livermore National Laboratory, P.O. Box 808, Livermore, California 94551

Received June 23, 2005

ABSTRACT: Polyaspartate domains are a prominent feature of proteins associated with biogenic carbonates and have been implicated in modifying crystal morphology through specific interactions with step edges. Here, we show that the morphology and growth kinetics of calcite are modified in a systematic way when a series of poly-L-aspartates, Asp_{1-6}, are introduced into solution. In-situ measurements of step propagation rates by atomic force microscopy reveal these effects are strongly chain-length dependent and specific to the crystallographically distinct, obtuse and acute step types. Direct observations of differential roughening and rounding of the step edges demonstrate that, while Asp_1 and Asp_2 have stronger effects on acute step edges, a crossover occurs for the longer $Asp_{4,5,6}$ peptides that preferentially affect obtuse steps. Independent analysis of Asp_n−step edge interactions by semiempirical quantum mechanical modeling gives estimates of aspartate−step edge binding energies and predicts that the crossover should occur at $n = 2$. The switch occurs because, upon Asp_n binding, the energy required to dehydrate acute steps is greater than that at the obtuse steps when $n = 3-6$. Step velocity measurements show that the concentration of Asp_n needed to stop growth scales exponentially and inversely with the calculated binding energies. A simple model of Asp_n adsorption to the steps is derived from these results. These findings suggest a process by which small fluctuations in primary structure in proteins can control calcite shape.

Introduction

The controlled synthesis of biominerals involves active constraints of crystal growth processes that result in functional structures beyond what is possible by passive growth in inorganic systems. Calcite, a polymorph of $CaCO_3$, represents an important model system for understanding these controlled mineralization processes due to its natural preponderance as a biogenic and inorganic carbonate mineral. An understanding of the molecular processes involved in calcite synthesis, and the means by which organic molecules mediate carbonate growth and shape, is important in addressing a broad range of questions including CO_2 sequestration,[1] industrial performance,[2] environmental remediation,[3] human pathology in pancreatic stones,[4] and paleoclimate analysis.[5]

Numerous studies have shown that proteins associated with carbonated mineral phases can determine the $CaCO_3$ polymorph that is generated, as well as morphology and orientation.[6−9] The controls of these proteins can be linked to their amino acid sequences and structures. However, the mechanisms by which their amino acid compositions and structures affect crystal growth are only beginning to be unraveled. When introduced in situ, specific proteins isolated from in vivo calcitic tissues demonstrate the ability to control $CaCO_3$ growth.[10,11] These proteins exhibit sequences with an unusually high fraction of acidic amino acids with carboxylate side chains, characterized by an abundance of glutamic and, especially, aspartic acid ($HOOC-CH_2-CH(NH_2)-COOH$).[12] The physical significance of this prevalence of aspartate residues among numerous biomineral-associated proteins remains in question.

Our previous work on aspartate has shown that single L or D enantiomers of aspartate residues (Asp_1) induce an asymmetry in the morphology of calcite growth hillocks.[13] These simple amino acids, however, are not representative of the long aspartate domains that are ubiquitous in proteins associated with calcitic tissues.[12] To better model the role(s) of these aspartate domains, this study focuses on how a series of synthetic linear poly-L-aspartates (Asp_n, $n = 1,2,4,5,6$) affect calcite mineralization during growth. The Asp_n compounds used here approximate well the size and linear sequence of the aspartate domains found in minerals associated aspartate-rich biomolecules (up to 50 mol % Asp content).[12] This study does not, however, attempt to reproduce the in vivo situation, which also involves the active control of the local ion concentrations, tailored biopolymeric scaffolds, and specific protein folding.[14] Rather, we provide information about plausible mechanisms of protein interactions with a crystal substrate.

Methods

Crystal Substrate and Solution Preparation. Natural calcite crystals (Chihuahua, Mexico locale) were cleaved to produce ~0.2 × 0.2 × 0.05 cm^3 fresh {104} faces as substrates for calcite growth. Calcite samples were used immediately upon cleaving, and a brief cleaning with a nitrogen jet was used to remove any debris. Growth solutions were prepared immediately before use from reagent grade calcium chloride ($CaCl_2 \cdot H_2O$), sodium bicarbonate ($NaHCO_3$), and sodium chloride (NaCl) dissolved in deionized (≥18 MΩ) and filtered water (0.2 μm). The chemistry of the baseline growth solution was carefully controlled with ionic strength fixed at 0.11 M, pH = 8.50, and a supersaturation of $\sigma = 0.92$. Supersaturation is defined as $\sigma = \ln(a_{Ca++}\, a_{CO3--}/K_{sp})$, using a $a_{Ca++}/a_{CO3--} \approx 1.0$, where "*a*" denotes the species activity calculated from Geochemist's Workbench (Urbana, IL) for specified parameters (pH, ionic strength, and temperature), and K_{sp} denotes the equilibrium solubility constant at 25 °C. Synthetic (Asp_n, $n = 1, 2, 4, 5, 6$) linear poly-α-aspartates 1 (D), 2 (D−D), and 4 (D−D−D−D) were obtained from Sigma-Aldrich (St Louis, MO), while Asp_5 (D−D−D−D−D) and Asp_6 (D−D−D−D−D−D) were supplied by American Peptide (Sunnyvale, CA). Asp_3 was not available commercially and therefore was not included in the experimental part of this study.

* Corresponding author. Telephone: (540) 231-1996. Fax: (540) 231-3386. E-mail: elhadj@vt.edu.
† Virginia Tech.
‡ University of South Alabama.
§ Lawrence Livermore National Laboratory.

10.1021/cg050288+ CCC: $33.50
Published on Web 09/21/2005

In-Situ AFM. During calcite growth, we imaged the steady-state morphology of atomic steps at constant supersaturation ($\sigma = 0.92$) for Asp_n concentrations of $0-10^{-1}$ M. Using established methods, calcite was overgrown onto the surface of a calcite seed crystal in an AFM flow-through cell (50 μL) that continuously supplied the input solution at a rate of 30 mL/h via a syringe pump.[15−17] Measurements of step speeds were conducted at room temperature using a Digital Instruments Nanoscope III (Veeco, Santa Barbara, CA) operating in Contact Mode. The AFM images were collected using scan rates of 5−20 Hz and a resolution of 512 × 512, while minimizing tip−surface force interactions during the flow-through of the growth solutions to avoid artifactual effects on step edge morphology and measured velocities.[17] Step velocity measurements were conducted for both the positive and the negative step edge directions on growth hillocks that had equilibrated with each type of growth solution.[17]

Circular Dichroism. The secondary structure of Asp_n was determined by collecting circular dichroism (CD) spectra with a Jasco J-720 spectropolarimeter (Essex, UK). Measurements were conducted in aqueous solutions of 0.01−0.1 M NaCl, pH = 8.5, adjusted with NaOH at room temperature and in a 0.1 mm sample cell. The CD spectra were obtained between 190 and 400 nm over a range of Asp_n dilutions ranging from 0.0325 to 0.5 mg/mL. The data were fitted using the CONTIN, SELCON, and CDSSTR algorithms[18] in addition to Kd2 software.[19] Background spectra were subtracted prior to fitting the data. Data fits that remained within suggested statistical tolerances were used to derive the secondary structures of Asp_n in terms of the nominal fractions of α-helix, β-strand, and random/folded conformations.

Molecular Modeling. The four step edges of {104} calcite surfaces were prepared using the CERIUS2 (version 4.8.1) surface builder (Accelrys, San Diego) from X-ray crystallographic data. Flexible ligand docking with simulated annealing was performed on the Asp_n/calcite system using cvff force field[20] parameters and an r-dependent dielectric ($r_{die} = 4$). Ions of the binding site were tethered to their lattice positions during docking and held frozen during subsequent optimizations because negligible surface relaxations, or reconstructions, are expected for such systems.[21,22] These initial calculations were performed on a Silicon Graphics Tezro workstation using Affinity-InsightII (version 2000) software (Accelrys, San Diego). Subsequent PM5 semiempirical quantum mechanics (MOPAC 2002, Fujitsu, Portland) optimizations were carried out on the most favorable binding orientations found via Affinity docking. PM5 calculations used the large molecule MOZYME algorithm of the CAChe (version 6.1) software package (Fujitsu, Portland). For the larger polypeptides ($n = 4-6$), inspection of the Affinity-docked structures led to identification of regular binding motifs, which were then applied to generate several initial structures for PM5 optimizations across the Asp_n series. During all PM5 energy minimizations, the ions of the crystal lattice were frozen, and a dielectric of 78.4 with an effective probe radius of 1 Å was used to emulate water as solvent. Also, hydrated stepped surfaces with 27−28 adsorbed water molecules were prepared, and PM5 optimizations were carried out. Superposition of the bound ligand orientations onto the hydrated calcite surfaces permitted us to identify displaced waters.[23]

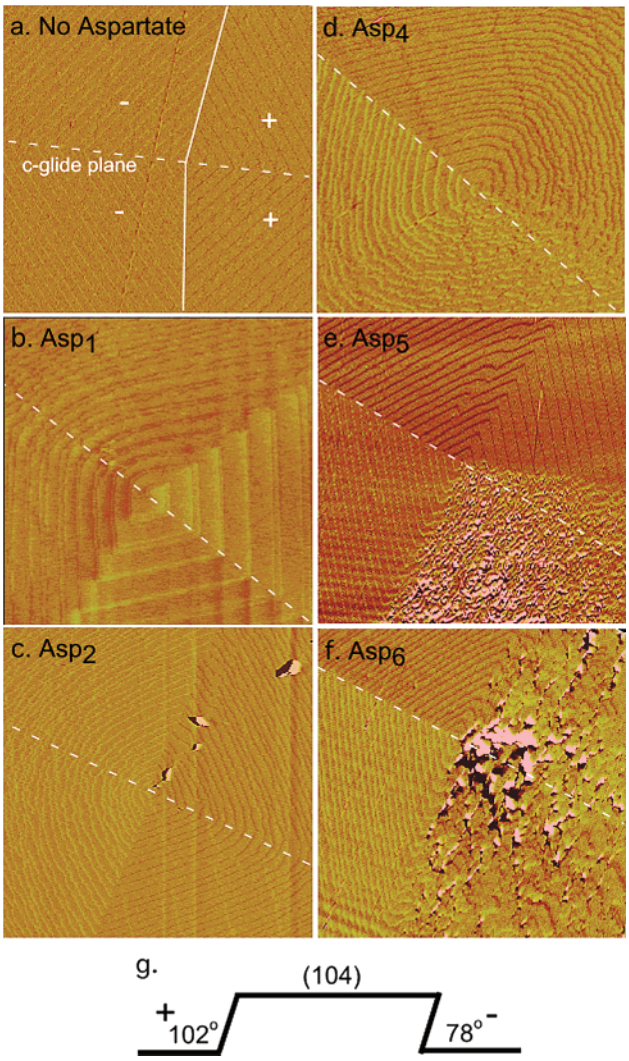

Figure 1. In-situ AFM images of calcite growth hillocks (3 × 3 μm). Steady-state hillock morphology in (a) the absence of Asp_n with c-glide plane and positive (obtuse) and negative (acute) steps as indicated; (b) in the presence of Asp_1 at 1.0×10^{-2} M; (c) Asp_2 at 1.0×10^{-4} M; (d) Asp_4 at 7.0×10^{-7} M; (e) Asp_5 at 1.3×10^{-6} M; (f) Asp_6 at 5.0×10^{-7} M. (g) Schematic cross section of the obtuse and acute step riser shows differences in step edge structure. Each observation was independently replicated at least three times for each Asp_n treatment.

Results and Discussion

Asp_n as a Morphological Switch. Observations of calcite growth in Asp_n bearing solutions by in-situ atomic force microscopy (AFM) isolated the effects of each peptide on calcite growth kinetics and provided insights into the mechanisms by which these impurities alter step edge morphology. As expected for the supersaturation used in these experiments, calcite growth in the absence of Asp_n occurred as the propagation of steps from dislocation sources (Figure 1a).[17] In these control solutions, the (positive) obtuse steps and (negative) acute steps exhibited straight edges that were symmetrically equivalent across the c-glide plane (Figure 1a and g).

For each experiment in which we introduced polyaspartate compounds, we monitored the early-stage changes in step morphology at near real-time. When low concentrations of the small, Asp_1 or Asp_2, molecules were introduced into the growth solution, step edges remained straight with increasing concentrations up to Asp_n concentrations of approximately $<10^{-3}$ and $<10^{-4}$ M, respectively. Within seconds of introducing Asp_1 or Asp_2 at these higher levels, the acute step edges roughened with a pronounced rounding at the intersections of step edges at the hillock corners (Figure 1b and 1c), and then the roughening propagates across the entire length of the step (Figure 1). These effects were clearly seen in time-lapse AFM images (data not shown). The obtuse steps remain relatively straight and unaffected by the presence of Asp_1 and Asp_2 in agreement with our previous findings.[13,24]

In contrast, when each of the longer Asp_4, Asp_5, or Asp_6 compounds were introduced into the growth solutions, the effects on step edges were exactly reversed such that roughening occurs to a much greater extent on the obtuse steps than on the acute (Figure 1d−f, respectively). Again, rounding is initiated at the intersection of the obtuse steps, and the onset of these morphological changes occurs at progressively lower Asp_n concentration with increasing n. For all peptides, further increases in Asp_n concentrations promote increased step roughening until the effects become apparent on all four step edges

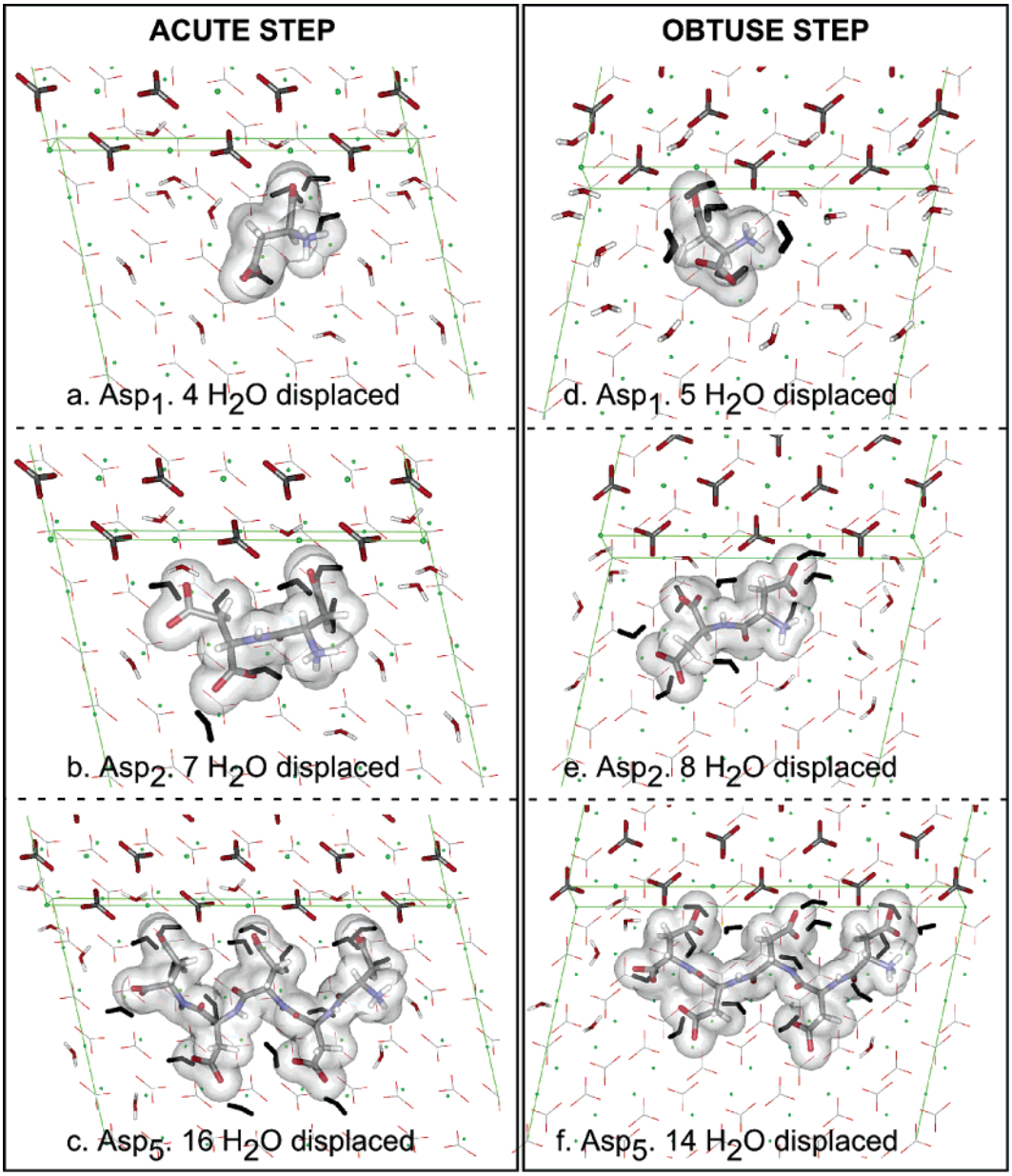

Figure 2. Computational model for a representative set of Asp_n binding to the hydrated right acute (a,b,c) and obtuse (d,e,f) calcite steps for Asp_1, Asp_2, and Asp_5. A green outline delineates the steps (Ca = green, C = gray, N = blue, O = red, H = white). The contrast in water molecules displaced by the binding of Asp_1 (a, d), Asp_2 (b, e), and Asp_5 (c, f) to the steps is shown, and the number of displaced H_2O molecules is depicted in black for emphasis. Asp_4 and Asp_6 also exhibit a greater number of water molecules displaced on the acute steps as compared to the obtuse steps (Asp_4, 14 acute and 13 obtuse; Asp_6, 19 acute and 18 obtuse).

at higher concentrations. Even so, the differential effects on acute versus obtuse edges remain and are always initiated at the corners of step edges for all Asp_n used. It is likely that the relatively higher interfacial energy in these areas of high curvature, where the atoms of the crystal structure tend to have lower coordination and thus have higher interfacial energy, favors both Asp_n binding at those sites and the observed initial changes in step morphology.

Model of Asp_n Binding to Step Edges. The *n*-specific effects of Asp_n on calcite growth can be understood from an independent model of aspartate−step edge interactions using semiempirical quantum mechanical methods. From initial computational searches, we were able to propose the unique binding configurations between Asp_n and the four individual steps, some of which are shown in Figure 2. The geometries of Asp_n−calcite interactions primarily involve the bridging of carboxylate groups across the step edge and surface calcium ions. In the case of acute step binding, the carboxylates tend to bind the calcium ions at step edges in a bidentate fashion. Additionally, there are favorable interactions between terrace Ca^{2+} ions and the carbonyl oxygens of the Asp_n peptide bonds, as well as hydrogen bonds between the amide hydrogens of Asp_n and surface carbonates.

Results of the computational model suggest that the mechanistic basis for the crossover in morphological effects with increasing chain-length arises from the energy cost of dehydrating the surface bound water molecules. The longer Asp_n ($n > 2$) have a larger "footprint" at acute step edges and, therefore, must displace more water molecules than at the obtuse step edges (Figure 2). This means the overall energy "penalty" for $Asp_{3,4,5,6}$ binding to the acute step is greater than for the obtuse step and thus favors $Asp_{3,4,5,6}$ binding to the obtuse step. For

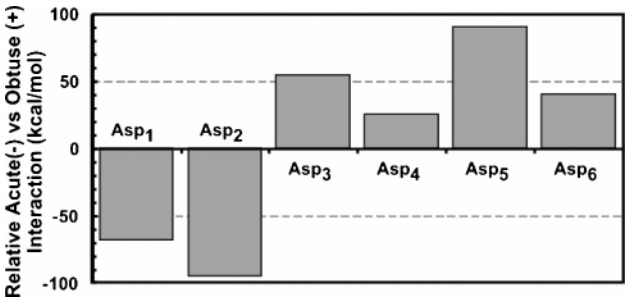

Figure 3. Calculated Asp_n relative interaction energies obtained by subtracting the binding energy to the obtuse step from that for the acute (see Methods for details). A negative interaction energy indicates favorable Asp_n binding to the acute steps for Asp_1 and Asp_2, while a positive value indicates favorable Asp_n binding to the obtuse steps for $Asp_{4,5,6}$.

example, in the case of Asp_5 (Figure 2), two additional water molecules are displaced on the acute side, resulting in a greater energy penalty for Asp_5 binding to the acute steps. In the case of Asp_1 and Asp_2, one additional water molecule is removed from the surface on the obtuse side after binding to the steps than is removed when binding to the acute steps (Figure 2). Without taking into account the displacement of adsorbed waters, binding to an acute step by carboxylate-containing Asp_n ligands is expected to be energetically more favorable than binding to an obtuse step due to the greater exposure of the Ca^{2+} ions along the acute step edge. We find this to be true across the entire Asp_n series, with acute step binding favored by about 50 kcal mol^{-1} (1 kcal = 4.18 kJ) for $n \geq 1$ when displacement of water is ignored. However, Figure 2 demonstrates that differences in the number of water molecules displaced exist between the acute and obtuse step edges, and we propose that this determines the Asp_n *n*-dependent step binding preferences.

Our assumption that the binding of Asp_n to step edges is dominant relative to terraces is validated by the contrast between the energy of binding to the steps and binding to the flat surface without contribution of the step. Calculated differences in binding energy for representative Asp_n conformations (data not shown) significantly favor binding to a step edge for all Asp_n species by ~30−150 kcal/mol, or about half the binding energy for terrace binding. As discussed later, this energy difference is especially important considering the exponential relationship between binding energy and the extent of surface coverage. It is thus expected that an overwhelming fraction of the Asp_n bound to the calcite surface will be located at the steps where calcite growth occurs.

The theoretical model gives an internally consistent picture of Asp_n interactions with step edges that also predicts the experimental data. For example, the crossover in the step-specific effects of Asp_n on step morphology at $n > 2$ (Figure 1) is supported by our estimates of the relative binding energies. By using the value determined from the Asp_n binding energy at the obtuse step, minus that at the acute step, which include water displacement penalties, the model similarly predicts a crossover between $n = 2$ and 3 (Figure 3). A previous computational study[23] also reported a water-induced reversal of acute versus obtuse binding for methanoic acid onto calcite.

The fitted circular dichroism (CD) spectra (data not shown) further delineate the modality of Asp_n binding to calcite by revealing that the conformations of the Asp_n in solution before binding were mostly random and compact before binding, with roughly 40 ± 15% of the chain in structured β and 10 ± 5% in α strand conformation. Our model calculations, however,

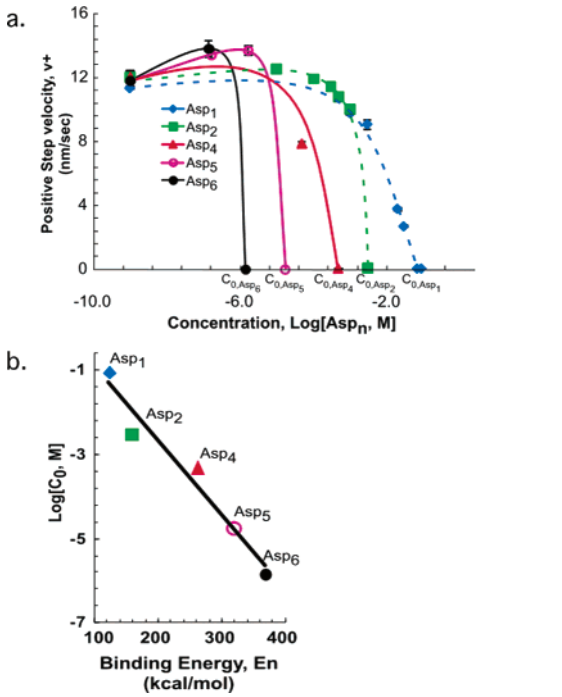

Figure 4. Kinetic measurements of obtuse (positive) step propagation rate versus Asp_n concentration (a). Acute (negative) step velocities exhibit the same dependence on aspartate concentrations (data not shown). The critical experimental concentrations required to halt growth, C_0, are plotted versus E_n, the calculated Asp_n binding energy to the calcite steps averaged over all steps (b). The ± error bars represent one standard deviation of measurements error ($n = 4-6$), and the correlation coefficient for a linear fit to the data was determined to be $R^2 = 0.954$.

suggest that, upon binding, the Asp_n is unfolded and extends to maximize binding. A similar unfolding upon binding was reported in a molecular dynamics model of the docking of short-chain peptides to calcite {104} faces.[25] Further, the fact that Asp_n conformations did not change with increased concentrations in solution, which would be expected when peptide aggregation occurs at higher concentrations, indicates that the Asp_n are not aggregated in solution and thus arrive at the steps as single independent units. We also determined that inter-aspartate interactions at calcite step edges were not significant because adsorption and desorption rates (derived below) can be correctly modeled by the law of mass action, which inherently assumes no inter-species interactions. Therefore, Asp_n-specific effects on step morphology and kinetics reflect changes in their individual size and direct interactions with the steps, rather than differences in intermolecular interactions and solution-phase configurations.

Effects of Asp_n on Growth Kinetics. In parallel with observations of step morphology, we measured the dependence of step propagation rates on Asp_n concentration (Figure 4a). Low concentrations of Asp_n cause small increases in calcite growth rate similar to the rate-modifying effects of the AP8 protein.[26] The most salient feature of Figure 4a, however, is the abrupt drop in step speed to $v = 0$ at a critical concentration C_0. The data show that C_0 is a strongly decreasing function of chain length. In other words, Asp_n becomes an increasingly potent step inhibitor with increasing n (Figure 4a). This is consistent with observations that the concentration of Asp_n required to affect step edge morphology is also inversely related to n.

A quantitative relationship between C_0 and Asp_n chain length can be derived by considering the dependence of site coverage,

θ, on Asp_n binding energy, E_n, to calcite step edges. The rate of change of θ is given by the difference between the attachment and detachment rates of Asp_n defined as R_a and R_d, respectively. Because the step speed is zero at C_0, the difference between R_a and R_d goes to zero and the coverage reaches equilibrium. That is, $d\theta/dt = R_a - R_d = 0$ at $C = C_0$, with $R_a = (1 - \theta)KC$ and $R_d = \theta\nu \exp(-bE_n/kT)$, where K is a rate constant, k is Boltzmann's constant, T is the absolute temperature, b is a dimensionless factor <1 that relates the desorption energy to the total binding energy E_n, and ν is the attempt frequency due to thermal fluctuations equal to h/kT where h is Planck's constant. While the coverage of Asp_n reaches equilibrium at $C = C_0$, the factor that determines when step motion is stopped is the fraction of blocked sites, which, for the same fractional coverage θ, is larger for longer chains and is given by the product, $f(n)\theta$, where $f(n)$ describes relationship between chain length and number of blocked sites (as Figure 2 shows, the dependence of $f(n)$ on n is weaker than linear). When C reaches the critical concentration, C_0, then $f(n)\theta$ reaches a critical fraction, F_0. The same relationships hold for F_0 as for θ at $C = C_0$. Setting the logarithm of R_a equal to that of R_d and using the above expressions for R_a and R_d above give:

$$\mathrm{Log}[C_0] = \mathrm{Log}[F_0\nu/(1 - F_0)K] - (b/kT)E_n \qquad (1)$$

Equation 1 shows explicitly that, to the extent that Log(K) and b are independent of n, Log[C_0] should be linear in E_n. Indeed, as Figure 4b shows, the experimentally measured values of C_0 have the predicted dependence on E_n. In principle, the intercept in Figure 4b contains information concerning both the rate coefficients, K, and the critical fractions, F_0. However, because an independent estimate of one is needed to extract the other, the current study cannot independently estimate either. From a linear fit to the data in Figure 4b and the expression for the slope of the line (b/kT) in eq 1, we estimate that $b = 10^{-2}$, which indicates that the energy barrier is ~1% of the total binding energy E_n.

It is noteworthy that the kinetic data are predicted by the model results when one considers the effect of chain length on Asp_n binding strength. Because each aspartate amino acid residue in the Asp_n molecule contributes additional binding energy, as the chain length increases, the binding strength increases linearly (Figure 4b), while the probability for desorption should decrease exponentially (eq 1). Thus, the rate of Asp_n turnover at the steps should be reduced and the coverage increased, reducing the solution concentration of Asp_n needed to inhibit step motion.

Conclusions

Our findings that peptide chain length confers specific differential and stereochemical binding to a mineral while also affecting growth dynamics suggest a new mechanism for mediating calcite morphology and other crystals grown in solution. This insight with simple peptides could indicate a means by which the primary structure of a more complex protein may also modify biomineral formation. The n-specific binding energies of Asp_n to calcite steps, when coupled to the local step dehydration, can produce crystallographically discriminating effects in peptide−mineral surface interactions, thereby opening the possibility that this type of growth regulation could be a plausible mechanism for stringent controls on both rates of formation and mineral shape.

Acknowledgment. This work was funded by the U.S. Department of Energy, Division of Chemical Sciences, Geosciences and Biosciences contract DE-FG02-00ER15112. This work was performed under the auspices of the U.S. Department of Energy by the University of California, Lawrence Livermore National Laboratory, under contract No. W-7405-Eng-48.

References

(1) Schulz, K. G.; Zondervan, I.; Gerringa, L. J. A.; Timmermans, K. R.; Veldhuis, M. J. W.; Riebesell, U. *Nature* **2004**, *430*, 673−676.
(2) Budair, M. O.; Khan, M. S.; Zubair, S. M.; Sheikh, A. K.; Quddus, A. *Heat Mass Transfer* **1998**, *34*, 163−170.
(3) Makarov, V. N.; Mazukhina, S. I.; Makarov, D. V.; Vasil'eva, T. N.; Kremenetskaya, I. P. *Russ. J. Inorg. Chem.* **2001**, *46*, 1646−1654.
(4) Moore, E. W.; Verine, H. J. *Am. J. Physiol.* **1987**, *252*, G707−G718.
(5) Elderfield, H.; Ganssen, G. *Nature* **2000**, *405*, 442−445.
(6) Addadi, L.; Weiner, S. *Proc. Natl. Acad. Sci. U.S.A.* **1985**, *82*, 4110−4114.
(7) Addadi, L.; Berman, A.; Moradianoldak, J.; Weiner, S. *Croat. Chem. Acta* **1990**, *63*, 539−544.
(8) Aizenberg, J.; Ilan, N.; Weiner, S.; Addadi, L. *Connect. Tissue Res.* **1996**, *35*, 17−23.
(9) Weiner, S. *Biochemistry* **1983**, *22*, 4139−4145.
(10) Aizenberg, J.; Albeck, S.; Weiner, S.; Addadi, L. *J. Cryst. Growth* **1994**, *142*, 156−164.
(11) Mann, S. *J. Mater. Chem.* **1995**, *5*, 935−946.
(12) Gotliv, B. A.; Kessler, N.; Sumerel, J. L.; Morse, D. E.; Tuross, N.; Addadi, L.; Weiner, S. *Chembiochem* **2005**, *6*, 304−314.
(13) Orme, C. A.; Noy, A.; Wierzbicki, A.; McBride, M. T.; Grantham, M.; Teng, H. H.; Dove, P. M.; DeYoreo, J. J. *Nature* **2001**, *411*, 775−779.
(14) Falini, G.; Fermani, S.; Gazzano, M.; Ripamonti, A. *J. Chem. Soc., Dalton Trans.* **2000**, 3983−3987.
(15) Land, T. A.; DeYoreo, J. J.; Lee, J. D. *Surf. Sci.* **1997**, *384*, 136−155.
(16) Teng, H. H.; Dove, P. M.; DeYoreo, J. J. *Geochim. Cosmochim. Acta* **1999**, *63*, 2507−2512.
(17) Teng, H. H.; Dove, P. M.; De Yoreo, J. J. *Geochim. Cosmochim. Acta* **2000**, *64*, 2255−2266.
(18) Sreerama, N.; Woody, R. W. *Anal. Biochem.* **2000**, *287*, 252−60.
(19) Andrade, M. A.; Chacon, P.; Merelo, J. J.; Moran, F. *Protein Eng.* **1993**, *6*, 383−390.
(20) Dauberosguthorpe, P.; Roberts, V. A.; Osguthorpe, D. J.; Wolff, J.; Genest, M.; Hagler, A. T. *Proteins* **1988**, *4*, 31−47.
(21) de Vries, S. A.; Goedtkindt, P.; Bennett, S. L.; Huisman, W. J.; Zwanenburg, M. J.; Smilgies, D. M.; De Yoreo, J. J.; van Enckevort, W. J. P.; Bennema, P.; Vlieg, E. *Phys. Rev. Lett.* **1998**, *80*, 2229−2232.
(22) Fenter, P.; Sturchio, N. C. *Geochim. Cosmochim. Acta* **1999**, *63*, 3145−3152.
(23) de Leeuw, N.; Cooper, T. *Cryst. Growth Des.* **2004**, *4*, 123−133.
(24) Teng, H. H.; Dove, P. M.; Orme, C. A.; De Yoreo, J. J. *Science* **1998**, *282*, 724−727.
(25) Gerbaud, V.; Pignol, D.; Loret, E.; Bertrand, J. A.; Berland, Y.; Fontecilla-Camps, J. C.; Canselier, J. P.; Gabas, N.; Verdier, J. M. *J. Biol. Chem.* **2000**, *275*, 1057−1064.
(26) Fu, G.; Qiu, S. R.; Orme, C. A.; Morse, D. E.; De Yoreo, J. J. *Adv. Mater.*, in press.

CG050288+